LAWRENCE
LIVERMORE
NATIONAL
LABORATORY

UCRL-CONF-201234

Temporal Characterization of a Picosecond Laser-Pumped X-ray Laser (for Applications)

J. Dunn, R.F. Smith, R. Shepherd, R. Booth, J. Nilsen, J.R. Hunter, and V.N. Shlyaptsev

November 26, 2003

SPIE – International Society for Optical Engineering conference on Soft X-ray Lasers and Applications V , San Diego, CA, August 3 – 8, 2003

Vol. 5197

Temporal Characterization of a Picosecond Laser-Pumped X-ray Laser (for Applications)

J. Dunn [1], R.F. Smith [1], R. Shepherd [1], R. Booth [1], J. Nilsen [1], J.R. Hunter [1], and V.N. Shlyaptsev [2]

[1] *Lawrence Livermore National Laboratory, Livermore, CA 94551*
[2] *Dept. of Applied Science, University of California Davis-Livermore, Livermore, CA 94551*

ABSTRACT

Compact soft x-ray laser sources are now used routinely for various applications primarily because of their high repetition rate, high photon fluence and short pulse duration characteristics. For some of these applications, for example interferometry of high density laser-produced plasmas, longer optical drive pulses, 6 – 13 ps (FWHM), have been implemented to maximize the x-ray output and coherence. It is therefore important to know the x-ray laser pulse length, shape and repeatability for these specific experiments as a baseline measurement but also to better understand the temporal behavior as a function of the pumping conditions in general. We report a detailed temporal characterization of the picosecond-driven 14.7 nm Ni-like Pd ion x-ray laser on the Compact Multipulse Terawatt (COMET) laser at LLNL using an ultrafast x-ray streak camera measurement of a horizontal slice of the near-field x-ray laser pattern. This is measured as a function of the chirped pulse amplification pumping laser conditions, including varying the pump pulse from 0.5 – 27 ps (FWHM), varying the plasma column length as well as investigating traveling wave (TW) and non-TW irradiation conditions.

Keywords: x-ray laser, transient gain, temporal measurements, x-ray streak camera

1. INTRODUCTION

Saturated output, picosecond-laser-driven tabletop x-ray lasers have been used and reported for several applications over the last year [1 – 3]. An accurate measurement of the x-ray pulse duration is essential for these applications. It can also give insight and further understanding of the mechanisms contributing to the population inversion. Recent temporal measurements of transient gain x-ray lasers driven by picosecond lasers have shown that x-ray laser pulse duration can be as short as 2 – 3 ps (FWHM) for the Ni-like Ag x-ray laser under certain pumping conditions [4, 5]. In all of these experiments a combination of two laser pulses are utilized where a long nanosecond pulse forms a pre-plasma that is further heated by a second, shorter picosecond, high intensity pulse [6]. Simulations have shown that very high, but short-lived gain is generated during and after the peak of the short pulse for collisional Ne-like and Ni-like ion x-ray lasers [7, 8]. Other x-ray laser experiments using the pre-pulse technique [9], where a lower intensity (2 – 10% of main intensity) is followed several nanoseconds later by the main 70 – 100 ps (FWHM) laser pulse have been performed on similar mid-Z Ag and Pd targets [10 – 12]. Those experiments indicate that x-ray laser pulses of 32 – 40 ps are generated and are 2 – 3 times shorter than the laser pumping pulse [10 – 12].

There are still unanswered questions that warrant more detailed experimental temporal measurements of transient gain x-ray lasers. It was shown previously in our laboratory that longer picosecond pumping pulses could give higher x-ray laser output with all other parameters remaining constant [13]. In addition, some of the x-ray laser applications at LLNL require that the x-ray laser source is optimized by using 6 or 13 ps pumping pulses [1] which is longer than at other laboratories [4, 5]. It is important to know what effect this has on the Ni-like Pd 14.7 nm x-ray laser pulse duration. Secondly, some general idea of how the x-ray laser pulse length scales with the picosecond laser pulse would be of great interest. We have investigated some of these issues in this work by using an ultrafast (500 fs time resolution) x-ray streak camera that was recently used for x-ray spectroscopy of 100 fs laser-heated thin foils [14]. We utilize a near-field imaging technique to study the 14.7 nm line either in 2-dimensions (2-D) and time-integrated using a charge-coupled device (CCD) camera or in 1-D with temporal resolution using the fast streak camera. The x-ray laser pulse duration is measured as a function of the chirped pulse amplification pumping laser conditions, including varying the pump pulse from 0.5 – 27 ps (FWHM), varying the plasma column length as well as investigating traveling wave (TW) and non-TW irradiation

conditions. The results presented here are primarily the determination of the x-ray laser duration as a function of the short pulse duration at a fixed delay of 700 ps peak-to-peak between the two laser pulses. A detailed comparison with simulations will be published at a later date. The effect of changing the pulse separation and other pumping conditions on the x-ray laser temporal and spatial properties, together with x-ray laser interferometry measurements of the pre-formed electron density profile, are presented by Smith *et al.* in these proceedings [15].

2. LASER AND EXPERIMENTAL DESCRIPTION

The Ni-like Pd 14.7 nm x-ray laser beam was generated using two laser beams at 1054 nm wavelength from the Compact Multipulse Terawatt (COMET) laser facility at LLNL and could be fired at a repetition rate of 1 shot every 4 minutes [16]. Saturated x-ray laser output in excess of 10 μJ was previously demonstrated with a combination of a 600 ps full width at half maximum (FWHM) long pulse and a 1.2 ps main heating pulse. The long pulse arrives first forming the pre-plasma and is then followed by the short pulse after a delay of 700 ps peak-to-peak. Some changes to the experiment have been implemented. The line focus is lengthened to 1.6 cm long, using a cylindrical lens and an on-axis paraboloid focusing optics, and polished Pd slab target up to a maximum length of 1.25 cm are irradiated. Traveling

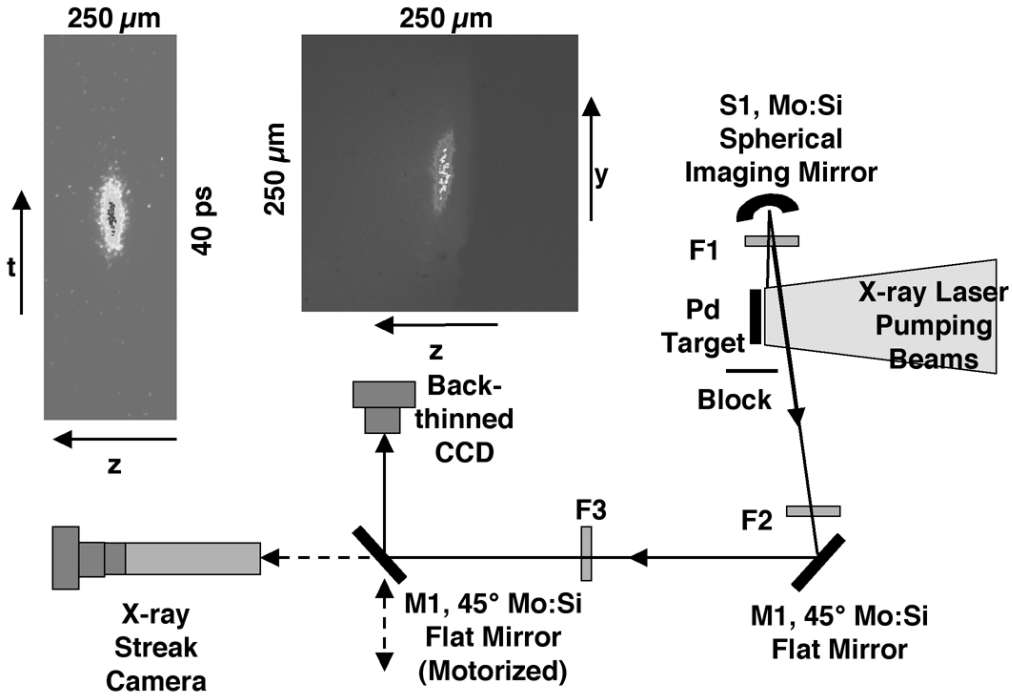

Figure 1: Experimental setup shows the near field x-ray laser imaging technique using multilayer-coated spherical mirror S1. Time-integrated, 2-D images (center inset picture) are recorded using back-thinned CCD camera with 45° multilayer optic M1 in. Time-resolved 1-D images (left inset picture) are recorded using the streak camera with M1 out. A combination of motorized thin foil filters (F1, F2, F3) are placed in the x-ray beamline to control the intensity.

wave line focus geometry was implemented before the focusing optics by using a high-reflectivity, 0° dielectric-coated reflection echelon consisting of seven flat vertical mirror segments. Each segment is offset by 0.12 cm relative to the adjacent mirror in the direction away from the optical axis of the laser drive beam. The stepped mirror produces a segmented line focus, each segment approximately 0.23 cm long, with each mirror segment offset to generate a delay of 7.8 ps relative to the next. Therefore, the TW line focus irradiation geometry is stepped and not continuous. Non-traveling wave geometry can be studied by replacing the TW mirror with a flat high reflectivity mirror [16]. Typically, the 14.7 nm x-ray laser output is enhanced along the direction of the TW by as much as two orders of magnitude. For this experiment, the long pulse was focused to ~150 μm (FWHM) with 1.25 ± 0.25 J energy on target (EOT). The short pulse energy was focused to 100 μm (FWHM) and contained 3.75 ± 0.25 J EOT. The short pulse duration was set by

adjusting the separation of the compressor gratings. Optimizing the compression gave the shortest pulse length of 500 fs, while de-tuning the compressor gave longer pulse durations of 1.75, 3.4, 6.7, 13.4, and 26.8 ps (FWHM).

Previous x-ray laser pulse measurements were performed using a streak camera with a grating spectrometer [4, 5]. As a consequence, the grating introduces a chirp of 1 – 2 ps on the measurements which has to be added to the instrumental temporal resolution of the streak camera. The experiment geometry here was chosen to satisfy a number of criteria. We wanted to spatially resolve the whole x-ray laser emission relative to the target as well as determine the spatial and temporal extent of the continuum emission. The temporal instrumental broadening effects were to be minimized. The experiment should have a similar setup to the x-ray laser beam line used for applications in order to determine the x-ray laser pulse under these conditions. The x-ray laser intensity should be carefully controlled to minimize instrument saturation effects. Finally, a sufficient number of shots were to be taken to ensure good statistics, to study repeatability and look for trends in the measurements. The experimental setup for the x-ray laser experiment is shown in Fig. 1. The x-ray laser output in the direction of the TW is imaged by a Mo:Si multilayer-coated spherical mirror (S1) with 11.75 cm focal length with high reflectivity centered on the 14.7 nm x-ray laser wavelength. This is relayed by a 45° Mo:Si multilayer-coated flat mirror (M1) onto either the streak camera or back-thinned CCD camera with 22 times magnification. Both detectors are at normal incidence to the x-ray laser beam and are placed equidistant to S1 to within ±0.05 cm. A second Mo:Si flat mirror (M2) is motorized to intercept the x-ray laser beam and direct it to either detector on a shot-to-shot basis. The center inset image in Fig.1 shows the time-integrated 2-D near-field image of the x-ray laser beam as it exits the end of the Pd target line focus. The streak camera is orientated in the horizontal direction, with the long axis of the entrance slit 100 μm × 2.5 cm (W × L) aligned along the z-axis, so that it samples a narrow, 1-D horizontal slice of the near-field image perpendicular to the Pd target. This is swept in time as shown in the left inset image in Fig. 1. Three filters F1, F2 and F3 are used in combination to control and attenuate (up to a maximum of 10^4) the x-ray laser fluence on the detectors. This allowed the x-ray laser to be studied at the threshold of lasing and in saturation.

3. X-RAY STREAK CAMERA CHARACTERIZATION

The streak camera was characterized during the experiment to measure the sweep speed, temporal response, spatial resolution, dynamic range and onset of space-charge saturation effects for exposure at x-ray laser photon energies. It is essential to know these parameters in order to operate the streak camera within the optimum regime. This camera has a measured temporal response of 500 fs (FWHM) using 100 fs pulses of 400 nm and 800 nm wavelength light with a Au photocathode [17]. Similar results have been confirmed with 0.7 – 0.8 nm x-rays [14]. For this experiment, the photocathode consisted of 120 nm CsI/75 nm Al coated on a thin, etched 40 nm Si_3N_4 window in a 250 μm Si wafer substrate. The extracted photoelectrons enter the drift tube and are subsequently focused with electron optics as they enter the sweep plate region. The swept electrons at the end of the streak tube are incident on a phosphor-coated fiber-optic. The light signal intensity from the phosphor is increased by a microchannel plate intensifier placed in contact at the back of the streak camera. The intensifier is operated in a low setting to minimize

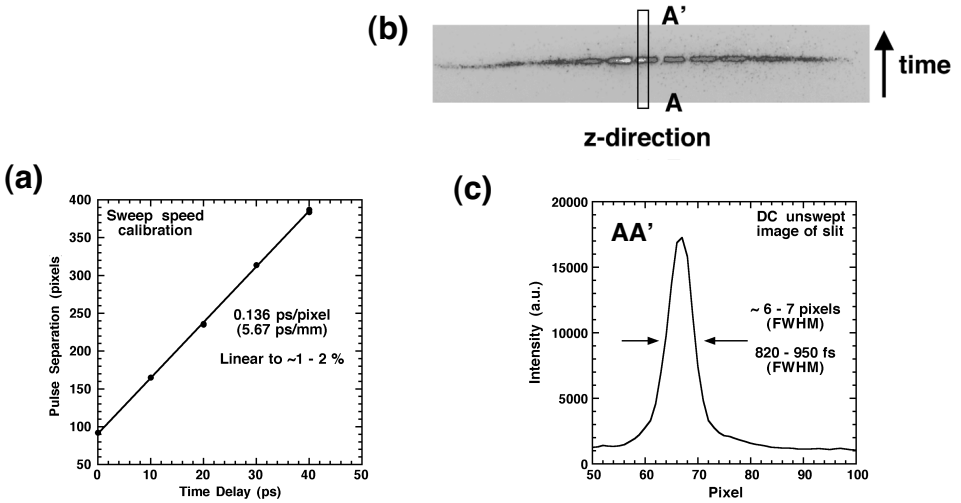

Figure 2: (a) Sweep speed calibration showing excellent linear response. (b) Image of photocathode slit for streak camera in focus mode (unswept). Note that a fiducial marker is placed in front of the photocathode to calibrate the 1-D spatial axis. (c) Lineout across image at AA' indicating finite slit width t_{DC} of 6 pixels (FWHM). This corresponds to 820 fs.

additional noise contributions to the image. A 2 times fiber-optic reducer demagnifies the image which is finally fiber-optic coupled to a CCD camera. The swept image is digitized at 16-bit resolution.

A Michelson type interferometer using a thin multilayer coated beamsplitter was introduced into the beam line to generate two x-ray laser pulses that were incident on the streak camera. Adjusting the length of one arm allowed the relative time delay between the pulses to be changed in order to calibrate the streak camera sweep speed in fast mode operation. Figure 2(a) shows the pixel position as a function of the time delay between the two pulses. The streak camera has measured sweep speed of 5.67 ps/mm (at the CCD camera) with a total time window of 101.8 ps. The sweep speed has excellent linearity to within ~1 – 2 %. The temporal resolution of the streak camera, to first order, will be determined by the slit width and image quality achieved with the electron focusing optics. Figure 2(b) shows the image of 14.7 nm x-rays illuminating the slit in DC or focus mode where the electrons are not being temporally swept. A lineout through the image at AA' shows the intensity profile with a minimum image width corresponding to finite slit width, t_{DC}, of 820 fs (FWHM), Fig. 2(c). This is the minimum time response for the streak camera and is slightly longer than the previously quoted 500 fs. This is attributed mainly due to the fiber-optic reducer, and some loss of spatial resolution, which was not used in the earlier experiments.

There are other factors that affect the streak camera temporal response when used in the swept mode. If the following assumptions are made: (a) The different effects have Gaussian pulse shape distributions; and (b) They all are independent, then the measured time response, t_{meas}, can be written as the quadratic summation where $t_{meas} = \{t_{DC}^2 + t_{ES}^2 + t_{SC}^2 + t_{XRL}^2\}^{1/2}$ [18]. The parameters t_{ES}, t_{SC}, and t_{XRL}, refer to the time dispersion due to the energy spread in photoelectrons, space-charge broadening due to coulombic repulsion of the electrons within the streak camera, and the x-ray laser temporal response, respectively [18]. The individual contributions listed above could be estimated. For example, the time dispersion component, t_{ES}, may be calculated from knowing the streak camera extraction field (15 kV) across the mesh to photocathode distance, the energy spread in photoelectrons, ΔE = 1.6 eV for CsI [19], and the time delay due to the different electron trajectories. However, it is not clear that the assumptions listed particularly (b) above are valid in all cases here and therefore how they combine. Space-charge effects observed with this streak camera result in a broadening of the pulse shape at the peak intensity producing a flattened non-Gaussian shape. This introduces a potential difficulty in the deconvolution of t_{XRL} from the measured pulse shapes. An alternative but simple method can be offered that addresses this issue. A reasonable estimate of the upper limit of the temporal resolution can be obtained by looking for the shortest measured pulse feature among all of the x-ray laser data. This involves analyzing hundreds of shots and looking for the shortest pulse width or rise time in the data. A very fast rise time of 1.4 ps (10 % – 90 % peak intensity) is observed in several shots for 6.7 ps pumping on a 0.6 cm target length. This pulse shape is shown in Fig. 3. It is not clear that this measured rise time is completely instrument limited in which case the streak camera response would be a partial and therefore smaller contribution. But nonetheless, in the absence of further information this upper limit can be placed on the streak camera temporal resolution with a high degree of confidence. We determine the streak camera resolution to be ~1 ps (FWHM) with an upper limit of 1.4 ps and a lower limit of 0.82 ps. These two limits are used to deconvolve the instrument response, in quadrature, from the measured values in the Experimental Results (Section 4). We add the caveat that this is for the streak camera operated at an incident x-ray fluence below the threshold for space-charge broadening effects.

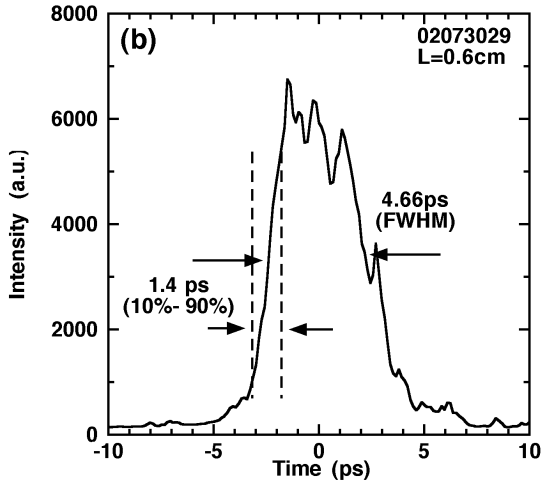

Figure 3: Measured x-ray laser pulse shape for 6.7 ps pump pulse irradiating a 0.6 cm Pd target, showing fast rise time of 1.4 ps (10 – 90% of peak intensity).

It is possible to carefully characterize the effect of space-charge and the resultant temporal instrument broadening using the large number of data shots available with a range of different x-ray fluences on the streak camera. Figure 4 shows a plot of measured x-ray laser pulse duration, t_{meas}, as a function of incident peak intensity. The data was recorded on one experimental day (21 recorded streak shots) all measured under similar pumping conditions of a 6.7 ps short pulse with TW geometry. It is clear from Fig. 4 that the measured x-ray pulse duration increases above a certain intensity threshold. Most of the data with peak intensity below 16000 a.u. are closely grouped around the mean value of 4.72 ps (FWHM) shown by the dashed horizontal line. However, data points with higher peak intensity also have broader pulse

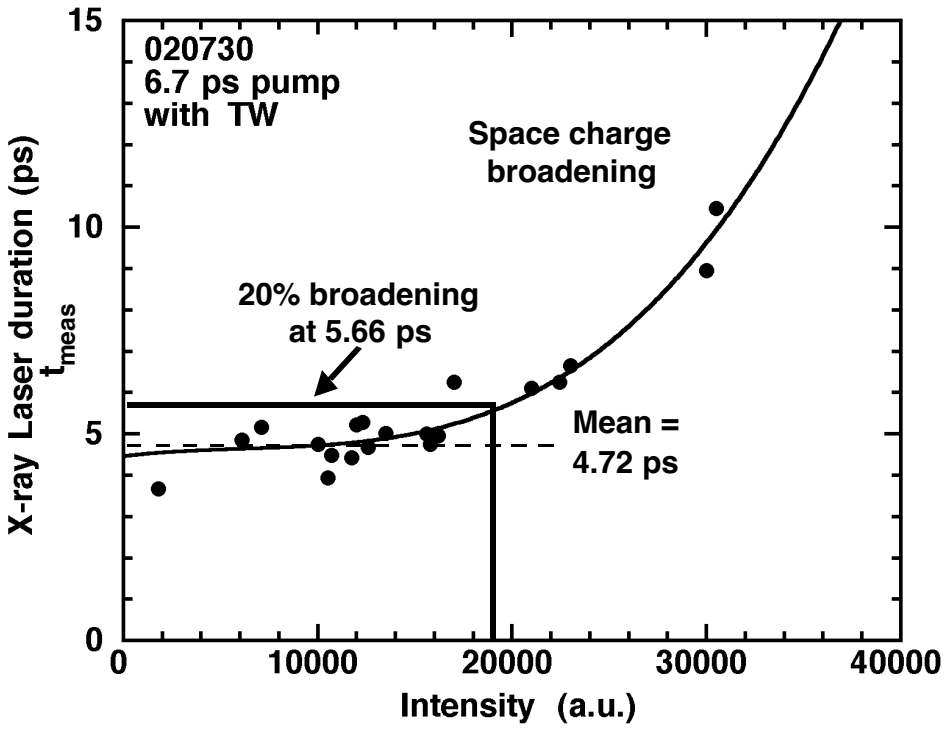

Figure 4: Measured x-ray laser pulse durations (FWHM), t_{meas}, as a function of peak intensity for 6.7 ps pumping pulse recorded under similar conditions. Points with intensity below 16000 a.u. are grouped around a mean value of 4.72 ps (FWHM). Above this intensity is the onset of temporal broadening of the measured pulse due to space-charge saturation inside streak camera. The threshold for the onset of saturation is determined at 20% broadening.

widths as high as 10 ps (see data points at 30000 a.u.). This dependence of t_{meas} *vs* I_{peak} has the classic shape of space-charge temporal broadening due to coulombic repulsion of the photoelectrons within the streak camera. It is beyond the scope of this work to go into further detail here other than to recognize the onset of the effect. This area has been reported extensively in the literature [20, 18] and has been determined in other recent x-ray laser experimental data [12]. We utilize the 20 % increase in broadening as the threshold (5.66 ps for this set of data) which corresponds to 19000 a.u. and ignore the data above this peak intensity because of space-charge saturation. This sets the effective dynamic range of the streak camera in the region of 40 – 50. For comparison, a cooled CCD camera can readily achieve a dynamic range of above 20000. The low intensity data point in Fig. 4 is also ignored because of the poor signal-to-noise ratio (SNR) for streaked images with low numbers of detected x-ray photons. The low signal shots tend to have very noisy profiles with spurious noise spikes that make the analysis difficult. So in this example for the data shown in Fig. 4, approximately 33% of all the data shots are rejected from the analysis because of space-charge or low SNR. This requires control of the incident x-ray laser fluence with the filter combination F1, F2, and F3 to achieve the best performance from the streak camera. It is worth noting that t_{meas} is the x-ray laser width with the instrument response included. After de-convolving the instrument response, the actual x-ray laser width t_{XRL} will be lower than t_{meas} by a small value, typically 0.1 – 0.2 ps, in most cases (see inset table in Fig. 6).

4. EXPERIMENTAL RESULTS

Several detailed parameter scans were performed and some of this work is presented here. It was possible to record low noise x-ray laser swept images and extract the pulse shapes, see Fig. 3. It was recently reported [4] that the rise and fall of the x-ray laser output is correlated with a change in the continuum emission and that this may be an indication of an extinction mechanism. The streak camera dynamic range limits the ability to simultaneously measure x-ray signals at different intensities, for example continuum emission and the x-ray laser pulse, under certain conditions. Figure 5 shows this for two different short pumping pulses where the x-ray filter attenuation has been adjusted to maintain the peak x-ray laser signal below the streak camera saturation level. The 600 ps pumping conditions and time delay between the two pulses, Δt, of 700 ps are similar. Fig. 5(a) shows the x-ray laser generated by a 500 fs laser pump focused on a 1.25 cm

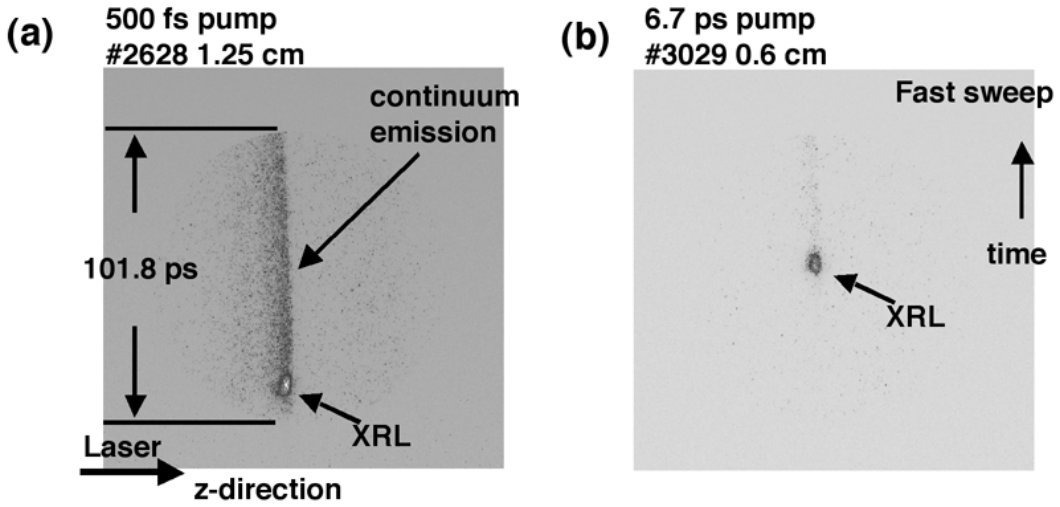

Figure 5: (a) X-ray laser streak image with short pulse pumping of 0.5 ps (FWHM) short pulse incident on a 1.25 cm target. Strong continuum emission is observed. (b) X-ray laser streak image with 6.7 ps (FWHM) on 0.6 cm target. Laser pump is incident from left and time is increasing up.

target. Figure 5(b) is a 6.7 ps laser pump focused on a 0.6 cm Pd target. Since this is also a 1-D near-field image the horizontal axis is perpendicular to the target and the laser pumps are incident from the left. The lower x-ray laser output for the pumping conditions in Fig. 5(a) allows the clear observation of the continuum emission starting just before the onset of the x-ray laser. The continuum emission lasts for more than 100 ps. The stronger x-ray laser output in Fig. 5(b), estimated to be in the gain saturation regime, requires more filtering and the continuum emission is at the threshold of detection. Nonetheless, Fig. 5 shows that it is possible with this experimental geometry to measure the spatially and temporally resolved x-ray laser and continuum emission. Figure 6 shows a plot of the measured x-ray laser pulse FWHM, t_{meas}, as a function of the short pumping pulse width. The long 600 ps pulse energy on target is kept constant at 1.25 ± 0.25 J and the delay between the pulses is 700 ps peak-to-peak. The short pulse laser energy EOT is also kept within the range of 3.75 ± 0.25 J. In all cases the traveling wave irradiation geometry was used. Five different short laser drives, varied from 0.5 ps to 26.8 ps, were used with 4 – 6 x-ray laser measurements for each pulse. The overall trend is clear that the x-ray laser pulse duration steadily increases with the duration of the laser drive, but only by a factor of 2.2× compared with the 50× increase in the laser drive. The inset table in Fig. 6 lists the laser drive, the measured x-ray pulse, t_{meas}, and the extracted x-ray laser duration, t_{XRL}, after using the instrumental width, t_{inst}, of 0.8 – 1.4 ps subtracted in quadrature. The error bars for column 2 and 3 are ± 1σ. The shortest x-ray laser pulse duration of 2.4 ± 0.1 ps are observed for drives below 1.75 ps. There are other similarly short x-ray laser pulses for longer 6.7 ps drive

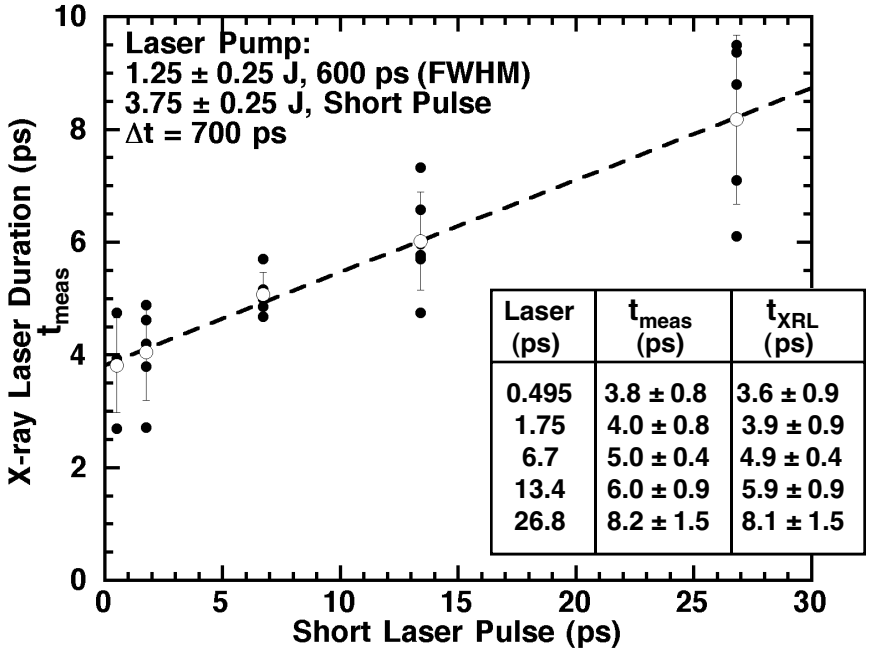

Laser (ps)	t_{meas} (ps)	t_{XRL} (ps)
0.495	3.8 ± 0.8	3.6 ± 0.9
1.75	4.0 ± 0.8	3.9 ± 0.9
6.7	5.0 ± 0.4	4.9 ± 0.4
13.4	6.0 ± 0.9	5.9 ± 0.9
26.8	8.2 ± 1.5	8.1 ± 1.5

Figure 6: Measured x-ray laser duration, t_{meas}, as a function of short pulse laser drive. Between 4 – 6 data points (closed circles) are recorded for each short pulse. The mean value (open circles) is shown with error bars of 1σ. The dashed line is a guide through the data points.

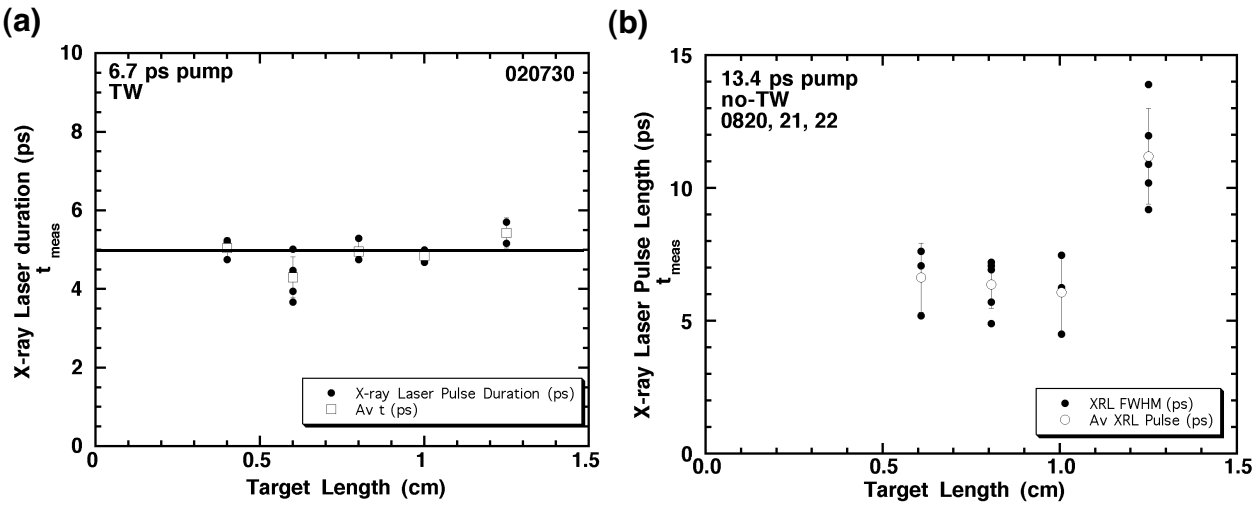

Figure 7: (a) Measured x-ray laser duration, t_{meas}, as a function of target length with TW for 6.7 ps pulse laser drive. Data points (closed circles) and mean value (open circles) with ± 1σ error bars. The horizontal line at 5 ps is a reference to guide the eye. (b) Measured x-ray laser duration, t_{meas}, as a function of target length with no-TW for 13.4 ps pulse laser drive. Data points (closed circles) and mean value (open circles) shown with error bars of 1σ.

pulses when the laser pump energy is reduced to close to the threshold for lasing. We note here that in both these cases the x-ray laser is not operating in the saturation regime. The overall values shown in Fig. 6 are slightly higher than RADEX simulations modeled with a perfect traveling wave [21]. It should be kept in mind that the traveling wave geometry implemented here is stepped and not continuous. Preliminary LASNEX and CRETIN simulations on the effect of a two-stepped TW line focus on the Ni-like Pd x-ray laser for 1 and 13 ps pumping indicate that there may be a 1.7× broadening of the x-ray laser pulse as a result of the imperfect traveling wave [22]. The stepped TW would be expected to converge to the pulse shape as the number of steps increased. Further analysis is in process. The effect of pulse duration as a function of target length with and without the traveling wave is shown in Fig. 7 (a) and (b). The results in Fig. 7(a) indicate that for a 6.7 ps laser pump with TW there is very little variation in the measured x-ray laser pulse duration and no strong trend showing broadening of the pulse in the saturation regime at longer target lengths. The 0.6 cm target gives a slightly shorter pulse duration of ~ 4 ps (FWHM). It is shown in Fig. 7(b) for 13.4 ps short pulse pump with no-TW, that the measured x-ray laser pulse durations are slightly longer (6 – 7 ps) for target lengths below 1 cm when compared the traveling wave case ~ 6 ps (Fig. 6). There does appear to be an increase in the pulse duration for 1.25 cm targets corresponding to a transit time of 42 ps. It would be expected to observe some de-coupling of the gain regions along the plasma length when the transit time is substantially longer than the gain lifetime for no TW irradiation. Shorter gain lifetimes associated with the shorter pumping pulses may exhibit this characteristic at earlier target lengths. In any case, the trend is shown that the traveling wave geometry consistently shortens the x-ray laser pulse duration and would also be beneficial for longer laser drives.

5. CONCLUSIONS

We have performed a comprehensive study of the x-ray laser pulse duration under different laser pumping conditions and with sufficient number of data points to achieve good statistics. An important part of the study was a careful characterization of the streak camera response to allow the correct interpretation and de-convolution of the x-ray laser pulse width and shape from the measured results. The x-ray streak camera temporal resolution is estimated to be 1.1 ± 0.3 ps (FWHM). An understanding of the onset of space-charge effects within the streak camera in order to minimize instrumental broadening effects while maximizing the signal-to-noise ratio is crucial. A smoothly decreasing x-ray laser pulse duration, from 8.1 to 3.6 ps, is observed when the short pulse pumping the inversion is decreased from 27 ps to 0.5 ps with traveling wave geometry. Although the pumping pulse varies by a factor of fifty the x-ray laser pulse duration varies by a factor of two. It has also been shown that the shortest x-ray laser pulse is observed in the range of 2.4 – 2.6 ps (FWHM) using short 0.5 or 1.75 ps laser drivers where the x-ray laser is not in saturation. X-ray pulses of a similar short

duration are observed on some shots using a 6 ps pumping laser where the incident pump energy is sufficiently low to take the x-ray laser well out of saturation. The pulse shape is observed to vary but many have a Gaussian shape. Typical pulse widths in the range of 4 – 6 ps are measured for many of the pumping conditions used for x-ray laser interferometry.

ACKNOWLEDGMENTS

The continued support and encouragement of Al Osterheld is greatly appreciated. The authors gratefully acknowledge the loan of a thin window, multilayer beam splitter from Philippe Zeitoun which was used to calibrate the sweep speed of the streak camera. This work was performed under the auspices of the U.S. Dept. of Energy by the University of California Lawrence Livermore National Laboratory under Contract No. W-7405-Eng-48.

REFERENCES

1. R.F. Smith, J. Dunn, J. Nilsen, V.N. Shlyaptsev, S. Moon, J. Filevich, J.J. Rocca, M.C. Marconi, J.R. Hunter, and T.W. Barbee, Jr., "Picosecond X-Ray Laser Interferometry of Dense Plasmas", *Phys. Rev. Lett*. **89**, 065004-1 (2002).
2. A.J. Nelson, J. Dunn, T.W. van Buuren, J. Hunter, R.F. Smith, O. Hemmers, and D. Lindle, "X-ray laser induced time-of-flight photoelectron spectroscopy", these proceedings (2003).
3. R.Z. Tai, K. Namikawa, M. Kishimoto, M. Tanaka, K. Sukegawa, N. Hasegawa, T. Kawachi, M. Kado, P. Lu, K. Nagashima, H. Daido, H. Maruyama, A. Sawada, M. Ando, and Y. Kato, "Picosecond Snapshot of the Speckles from Ferroelectric $BaTiO_3$ by Means of X-Ray Lasers", *Phys. Rev. Lett*. **89**, 257602-1 - 4 (2002).
4. A. Klisnick, J. Kuba, D. Ros, R. Smith, G. Jamelot, C. Chenais-Popovics, R. Keenan, S.J. Topping, C.L.S. Lewis, F. Strati, G.J. Tallents, D. Neely, R. Clarke, J. Collier, A.G. MacPhee, F. Bortolotto, "Demonstration of a 2-ps transient x-ray laser", P.V. Nickles, *Phys. Rev. A*. **65**, 033810 (2002).
5. Y. Abou-Ali, G.J. Tallents, M. Edwards, R.E. King, G.J. Pert, S.J. Pestehe, F. Strati, R. Keenan, C.L.S. Lewis, S. Topping, O. Guilbaud, A. Klisnick, D. Ros, R. Clarke, D. Neely, M. Notley, and A. Demir, "Measurement of the duration of X-ray lasing pumped by an optical laser pulse of picosecond duration", *Opt. Comm.* **215**, 397 (2003).
6. Yu.V. Afanasiev and V.N. Shlyaptsev, "Formation of a population inversion of transitions in Ne-like ions in steady-state and transient plasmas", *Sov. J. Quant. Electron.* **19**, 1606-1612 (1989); V.N. Shlyaptsev, P.V. Nickles, T. Schlegel, M.P. Kalashnikov, and A.L. Osterheld, "Table-top x-ray laser pumped with subnanosecond and picosecond pulses", *SPIE Int. Soc. Opt. Eng. Proc.* **2012**, 111-118 (1993).
7. P.V. Nickles, V.N. Shlyaptsev, M. Kalachnikov, M. Schnürer, I. Will, and W. Sandner, "Short Pulse X-ray Laser at 32.6 nm Based on Transient Gain in Ne-like Titanium", *Phys. Rev. Lett.* **78**(14), 2748-2751 (1997).
8. J. Dunn, A.L. Osterheld, R. Shepherd, W.E. White, V.N. Shlyaptsev, and R.E. Stewart, "Demonstration of X-ray Amplification in Transient Gain Nickel-like Palladium Scheme", *Phys. Rev. Lett.* **80**, 2825-2828 (1998).
9. J. Nilsen, B. MacGowan, L.B. DaSilva, J.C. Moreno, "Prepulse technique for producing low-Z Ne-like x-ray lasers", *Phys. Rev. A*, **48**, 4682-4685, (1993).
10. J. Zhang, A.G. MacPhee, J. Nilsen, J. Lin, T.W. Barbee, Jr., C. Danson, M.H. Key, C.L.S. Lewis, D. Neely, R.M.N. O'Rourke, G.J. Pert, R. Smith, G.J. Tallents, J.S. Wark, and E. Wolfrum," Demonstration of Saturation in a Ni-like Ag X-Ray Laser at 14 nm", *Phys. Rev. Lett.* **78**(20), 3856 – 3860 (1997).
11. S. Sebban, H. Daido, N. Sakaya, Y. Kato, K. Murai, H. Tang, Y. Gu, G. Huang, S. Wang, A. Klisnick, Ph. Zeitoun, F. Koike, and H. Takenaka, "Full characterization of a high-gain saturated x-ray laser at 13.9 nm", *Phys. Rev. A*. **61**, 043180-1 – 043180-9 (2000).
12. M. Braud, C. Siegel, J.E. Balmer, and J. Nilsen, "Near-Field Spatial Imaging and Time-Resolved Measurements of the Ni-like Palladium Soft X-ray Laser", *X-ray Lasers 2002*, ed. J.J. Rocca, J. Dunn, and S. Suckewer, AIP Conference Series Vol. 641 (AIP, New York, 2002), 154-159.
13. J. Dunn, A. L. Osterheld, J. Nilsen, J.R. Hunter, Y. Li, A. Ya. Faenov, T.A. Pikuz, and V.N. Shlyaptsev, "Saturated output tabletop x-ray lasers", *X-ray Lasers 2000*, ed. G. Jamelot, C. Möller, and A. Klisnick, *J. Phys. IV* **11**, (EDP Sciences, France, 2001) Pr2-19.
14. P. Audebert, R. Shepherd, K. B. Fournier, O. Peyrusse, D. Price, R. Lee, P. Springer, J.-C. Gauthier, and L. Klein, "Heating of Thin Foils with a Relativistic-Intensity Short-Pulse Laser", *Phys. Rev. Lett.* **89**, 265001-1 - 4 (2002).

15. R.F. Smith, J. Dunn, J. Filevich, S.J. Moon, J. Nilsen, R. Keenan, V.N. Shlyaptsev, J.J. Rocca, J.R. Hunter, R. Shepherd, R. Booth, and M. Marconi, "Improved energy coupling into the gain region of the Ni-like Pd transient collisional x-ray laser", these proceedings (2003).
16. J. Dunn, Y. Li, A.L. Osterheld, J. Nilsen, J.R. Hunter, V.N. Shlyaptsev, "Gain Saturation Regime for Laser-Driven Tabletop, Transient Ni-Like Ion X-Ray Lasers", *Phys. Rev. Lett.* **84**, 4834 (2000).
17. R. Shepherd, R. Booth, private communication (2002).
18. M.M. Murnane, H.C. Kapteyn, and R.W. Falcone, "X-ray streak camera with 2 ps response", *Appl. Phys. Lett.* **56**, 1948 (1990).
19. B.L. Henke, J. Liesengang, and S.D. Smith, "Soft-x-ray-induced secondary-electron emission from semiconductors and insulators: Models and measurements", *Phys. Rev. B* **19**, 3004 (1979).
20. R. Kalibjian, "Space charge temporal broadening effects in streak-camera tubes", *Proc. 13th Int. Cong. on High-speed Photography and Photonics*, Tokyo (1978); University of California, Lawrence Livermore Laboratory Report UCRL-80922 (1978).
21. V. N. Shlyaptsev *et al*, these proceedings (2003).
22. J. Nilsen *et al*, these proceedings (2003).